Regional staging of white matter signal abnormalities in aging and Alzheimer's disease

Emily R. Lindemer[a,b,c,*], Douglas N. Greve[b,c], Bruce R. Fischl[a,b,c,d], Jean C. Augustinack[b,c], David H. Salat[b,c,e], for the, Alzheimer's Disease Neuroimaging Initiative:

[a] Harvard-MIT Division of Health Sciences and Technology, Cambridge, MA, USA
[b] Athinoula A. Martinos Center for Biomedical Imaging, Charlestown, MA, USA
[c] Department of Radiology, Massachusetts General Hospital, Harvard Medical School, Boston, MA, USA
[d] Computer Science and Artificial Intelligence Laboratory (CSAIL), Massachusetts Institute of Technology (MIT), Cambridge, MA, USA
[e] Neuroimaging Research for Veterans (NeRVe) Center, VA Boston Healthcare System, Boston, MA, USA

ARTICLE INFO

ABSTRACT

White matter lesions, quantified as 'white matter signal abnormalities' (WMSA) on neuroimaging, are common incidental findings on brain images of older adults. This tissue damage is linked to cerebrovascular dysfunction and is associated with cognitive decline. The regional distribution of WMSA throughout the cerebral white matter has been described at a gross scale; however, to date no prior study has described regional patterns relative to cortical gyral landmarks which may be important for understanding functional impact. Additionally, no prior study has described how regional WMSA volume scales with total global WMSA. Such information could be used in the creation of a pathologic 'staging' of WMSA through a detailed regional characterization at the individual level. Magnetic resonance imaging data from 97 cognitively-healthy older individuals (OC) aged 52–90 from the Alzheimer's Disease Neuroimaging Initiative (ADNI) study were processed using a novel WMSA labeling procedure described in our prior work. WMSA were quantified regionally using a procedure that segments the cerebral white matter into 35 bilateral units based on proximity to landmarks in the cerebral cortex. An initial staging was performed by quantifying the regional WMSA volume in four groups based on quartiles of total WMSA volume (quartiles I–IV). A consistent spatial pattern of WMSA accumulation was observed with increasing quartile. A clustering procedure was then used to distinguish regions based on patterns of scaling of regional WMSA to global WMSA. Three patterns were extracted that showed high, medium, and non-scaling with global WMSA. Regions in the high-scaling cluster included periventricular, caudal and rostral middle frontal, inferior and superior parietal, supramarginal, and precuneus white matter. A data-driven staging procedure was then created based on patterns of WMSA scaling and specific regional cut-off values from the quartile analyses. Individuals with Alzheimer's disease (AD) and mild cognitive impairment (MCI) were then additionally staged, and significant differences in the percent of each diagnostic group in Stages I and IV were observed, with more AD individuals residing in Stage IV and more OC and MCI individuals residing in Stage I. These data demonstrate a consistent regional scaling relationship between global and regional WMSA that can be used to classify individuals into one of four stages of white matter disease. White matter staging could play an important role in a better understanding and the treatment of cerebrovascular contributions to brain aging and dementia.

1. Introduction

White matter signal abnormalities (WMSA; also commonly referred to as 'white matter hyperintensities of presumed vascular origin') (Wardlaw et al., 2013a; Benedictus et al., 2014; Wardlaw et al., 2013b) as detected on magnetic resonance imaging (MRI) (Lindemer et al., 2015; Fazekas et al., 1988; Wei et al., 2002) are a common pathology found in the aging brain. To date, the integration of WMSA into an understanding of both normal and diseased brain aging has been challenging. Prior studies have demonstrated that WMSA are associated with a range of altered neurological and psychological profiles and contribute to the profile of dementia in individuals with compounded neurological disease (de Leeuw et al., 2001; Frisoni et al., 2007; Grueter and Schulz, 2012; Brickman et al., 2009a; Brickman et al., 2009b; DeCarli et al., 2005; Iadecola, 2013; Yoshita et al., 2006; de Groot et al., 2002; de Groot et al., 2001), yet they are often treated as a benign comorbidity of aging due to their high prevalence of 80–95% in older adults (de Leeuw et al., 2001; Dufouil et al., 2001; Longstreth,

* Corresponding author at: Athinoula A. Martinos Center for Biomedical Imaging, 149 13th St. Suite 2301, Charlestown, MA 02129, United States.
E-mail address: lindemer@mit.edu (E.R. Lindemer).

1998). In order to better understand the development of WMSA without the complications of concurrent cognitive impairments, the aim of the current study is to outline a staging procedure for WMSA in cognitively healthy older adults that can be applied to disease populations such as Alzheimer's disease (AD) and mild cognitive impairment (MCI) to determine how WMSA involvement relates to disease state.

Visual rating scales exist for describing the degree of WMSA within an individual (Fazekas and Chawluk, 1987; Scheltens et al., 1993). These scales have been useful in ranking individuals based primarily on the degree of periventricular compared to deep WMSA. While individual variation exists, imaging studies have demonstrated that WMSA generally first appear and are most prominent in periventricular areas when total lesion burden is low, but they progressively expand to include white matter distal to the ventricles and proximal to the cortex with greater disease burden (Zimmerman et al., 1986; Spilt et al., 2006). It is still unclear, however, whether or not aging individuals show a stereotypical pattern of WMSA development. This study investigates whether there exists a consistent relationship between global and regional WMSA burden and uses this information in the quantitative staging of white matter disease based on vulnerable brain regions.

Here we used an approach to perform an individual staging of WMSA that is inspired from prior neuropathological studies that quantify the degree of regional pathology in conditions such as Alzheimer's disease by sorting individuals based on the severity of the given pathology and determining if a spatial pattern emerges (Braak and Braak, 1991; Augustinack et al., 2012). This creation of a WMSA staging procedure is limited to cognitively healthy older adults enrolled in the Alzheimer's Disease Neuroimaging Initiative to avoid complications of comorbid neurodegenerative processes. In addition to this staging procedure, we devise a method to study the relationship between regional and global WMSA burden in order to understand how the WMSA burden in different regions of the WM scales with total WMSA, demonstrating specific regional vulnerabilities to WMSA. To provide an example of this method's utility, the final staging procedure is then applied to individuals with AD and MCI to determine the relationship between disease prevalence and WMSA stage.

2. Methods

2.1. Data

Data used in the preparation of this article were obtained from the Alzheimer's Disease Neuroimaging Initiative (ADNI) database (adni.loni.usc.edu). The present study used data from the ADNI-1 database. Ninety-seven individuals were selected who had no present or history of cognitive impairment and no history of stroke. Data were selected based on the availability of images that had been already locally processed with FreeSurfer and limited to datasets with available T1-weighted, T2-weighted, and proton density (PD)-weighted images for WMSA processing. Demographic data such as age, sex, years of education, history of hypertension, history of endocrine-metabolic disorder, and Mini Mental State Examination (MMSE) scores were additionally acquired from the ADNI database.

Three diagnostic groups were used in this study: older controls (OC, n = 97), mild cognitive impairment (MCI n = 121), and Alzheimer's disease (AD n = 127). Briefly, all MCI participants have reported a subjective memory concern either autonomously or via an informant or clinician but do not have significant levels of impairment in other cognitive domains and have essentially preserved activities of daily living with no signs of dementia (i.e., all MCI individuals are amnestic MCI only). AD participants were evaluated and met the National Institute of Neurological and Communicative Disorders and Stroke/Alzheimer's Disease and Related Disorders Association criteria for probable AD. Through this evaluation process, ADNI aims to reduce the risk of including subjects with vascular and other types of dementia. All individuals in the MCI group were within three years of converting to AD as

determined by longitudinal ADNI follow-up data. Creation of the staging methods was performed solely with OC data, and the MCI and AD groups were only used in the final analyses after secondary staging cut-off values were chosen.

2.2. MRI acquisition

All data were acquired on a 1.5-T scanner at rigorously validated sites, which all followed a previously described standardized protocol (Jack et al., 2008). The protocol included a high-resolution, T1-weighted sagittal volumetric magnetization prepared rapid gradient echo sequence and axial PD and/or T2-weighted fast spin echo sequence. The ADNI MRI core optimized the acquisition parameters of these sequences for each make and model of scanner included in the study. All scanner sites were required to pass a strict scanner validation test before being allowed to scan ADNI participants. Additionally, each scan of ADNI participants included a scan of the phantom, which was required to pass additional strict validation tests.

2.3. MRI preprocessing

Each individual's T1-weighted MRI was processed using FreeSurfer's main recon-all processing stream with a recently described extension for the segmentation of WMSAs (Lindemer et al., 2015). Cortical reconstruction and volumetric segmentation was performed using FreeSurfer (surfer.nmr.mgh.harvard.edu/, version 5.1). The technical details of these procedures are described in prior publications (Dale and Sereno, 1993; Dale et al., 1999; Fischl and Dale, 2000; Fischl et al., 1999; Fischl et al., 2001; Fischl et al., 2002; Fischl et al., 2004a; Fischl et al., 2004b; Han et al., 2006; Jovicich et al., 2006).

2.4. WMSA segmentation

Images were processed with an automatic WMSA segmentation stream that has been previously described (Lindemer et al., 2015). Briefly, this procedure performs intensity normalization of an individual's T1-, T2- and PD-weighted images using a multimodal atlas, and segments WMSA from normal-appearing white matter (NAWM) using a multimodal Gaussian classifier as well as individual-based heuristics.

The WM was divided into 70 regions of interest (ROIs) that encompassed the entire subcortical WM as well as the periventricular WM as described previously (Salat et al., 2009). These ROIs were automatically created during FreeSurfer's recon-all processing stream, and correspond to the WM areas below the surface of the anatomically-defined cortical gray matter areas. ROIs were then combined across hemispheres for a total of 35 final ROIs, as WMSA have been shown to be a generally symmetrical pathology (Wardlaw et al., 2013a). For each ROI, the WMSA burden was calculated in three different ways. First, the raw volume of WMSA in each ROI was calculated. Second, due to the known decrease in WM volume with increasing age (Salat et al., 2009), the WMSA volume as a percent of the individual's native space total WM volume (NAWM + WMSA) was also calculated. Finally, WMSA volume as a percent of a standard atlas ROI's total WM was calculated to account for the possibility that atrophy of WMSA and NAWM regions occurred at differing rates. All three methods generated nearly identical staging results, and therefore the only metric that is fully presented here is WMSA as a percent of the individual's total native space WM volume.

2.5. Quartile-based staging

After WMSA segmentation, the 97 OC individuals were sequentially ordered based on total global WMSA volume (rank ordered from lowest to highest WMSA volume) for an initial/preliminary staging. Four stages were defined by dividing individuals into simple quartiles corresponding to those with the lowest total WMSA (Quartile I, n = 25), mid-low

total WMSA (Quartile II, n = 25), mid-high total WMSA (Quartile III, n = 25), and highest total WMSA (Quartile IV, n = 22) (Fig. 1, image and first dashed box). Using quartiles is somewhat arbitrary however we found similar results when using tertiles, quartiles, and quantiles. Quartiles were settled on as a final choice as it allowed a compromise between statistical power and visualization of subtler differences between stages for spatial and temporal characterization. The mean WMSA as a percent of total WM volume for each of the 35 FreeSurfer ROIs was calculated for each of the four quartiles. For visualization purposes, these mean values were mapped onto their corresponding cortical surface gyral regions based (Fig. 1, image).

As with neuropathological studies (Braak and Braak, 1991; Augustinack et al., 2012; Arnold et al., 1991), we infer staging based on cross-sectional information and use regional scaling relationships with total WMSA burden as the basis of our this procedure. This is appropriate for the given study as age-associated WMSA volume has been demonstrated to be non-decreasing with longitudinal data (Erten-Lyons et al., 2013; Maillard et al., 2014) and therefore a staged process can be inferred cross-sectionally.

2.6. Regional scaling

We are seeking a way to quantify how the WMSA burden in a given ROI scales with global burden. To do this, we first performed an ANOVA testing for a difference across the four quartiles for each of the 35 ROIs. As the quartiles were determined based on global WMSA, a high F-value indicates that the ROI's WMSA load strongly scales with global WMSA load. Next, we clustered the ROIs into three groups based on F-value using a k-means (k = 3) algorithm. These three progression clusters correspond to (Wardlaw et al., 2013a): non-scaling ROIs: low F-valued ROIs (Benedictus et al., 2014), mid-scaling ROIs (middle F-values), and (Wardlaw et al., 2013b) High-scaling ROIs (high F-values). The identity of the ROIs in the progression clusters gives an idea of how WMSA burden spatially manifests across the brain, which is the goal of this study (Fig. 1, second dashed box).

To evaluate our scaling method statistically, we employed a permutation-knockout test to determine whether the spatial scaling pattern that we found was likely to appear by chance. Under the null hypothesis, no ROI scales higher than any other ROI with global WMSA load. In each permutation, we randomly reassigned the WMSA volume of an ROI for a given subject to another ROI in that subject, repeating for all subjects. The data was then staged, and the F-value was computed for the ROI that had the highest F-value in the real data. This was repeated 10,000 times. The p-value for this top-ranking ROI was then computed as the number of times out of 10,000 that the permutation F-value exceeded the F-value in the true data. The same procedure was repeated for the ROI with the second highest F-value except that the highest ranking ROI was removed (knocked out). This was repeated for all high-scaling ROIs, knocking out the previous highest-ranking ROI. If the pattern found in the true data is likely to be seen by chance, then the p-values should be relatively high. Note that we cannot simply use the p-values computed from the ANOVA F-test they would be biased by the staging procedure.

To test reliability, 10,000 permutations were performed in which random subsamples of 64 individuals were chosen for each permutation. The above methodology was then applied to each subsample, by first ordering the 64 subjects, splitting them into quartiles, and performing ROI-based ANOVAs on each ROI. F-stats from the ANOVAs were then clustered, and the number of times out of 10,000 that each ROI was placed into its true scaling cluster, as determined from the full dataset, was calculated as its reliability score.

2.7. Staging cut-offs

To provide a quantitative guideline by which to stage future individuals, we developed a cut-off-based staging system using information from the quartile-based staging. This was done by identifying high-scaling ROIs from the quartile-based analyses and working backwards from Stage IV to Stage I. More specifically, the high-scaling ROI that showed the greatest WMSA difference between the third and fourth quartiles was first identified. The mean and standard deviation of the WMSA burden in this ROI in the fourth quartile were used to determine a cut-off value (cut-off 1). This was then repeated with high-scaling ROIs that differed significantly between the second and third quartiles (cut-off 2), and the first and second quartiles (cut-off 3). These three cut-off values were then used to re-stage all individuals in the OC group. F-tests for the equality of variances between quartile-based and final stages for OC
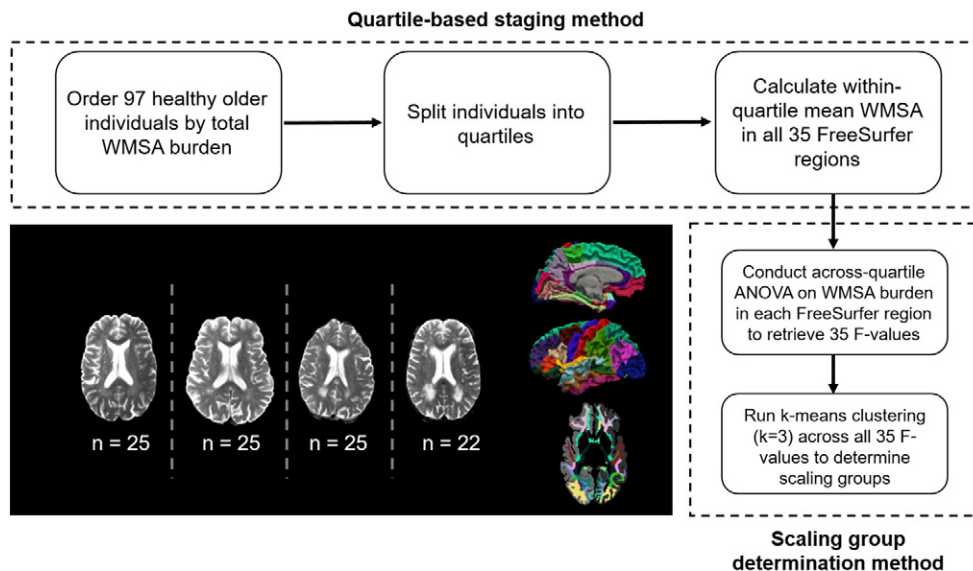

Fig. 1. Visual representation of staging and scaling methods. In the scaling method, the three clusters from the k-means cluster analysis refer to ROIs that are non-scaling (low F-values), low-scaling (middle F-values), and high-scaling (high F-values) with global WMSA burden. Image shows examples of an individual in each of the four quartiles going from low to high total WMSA burden as well as FreeSurfer WM parcellations projected onto the brain's surface.

individuals in each ROI were performed to determine if within-stage variance decreased using the final staging method.

2.8. Statistical analyses

Differences across quartiles in continuous demographic variables such as age and years of education were assessed using a one-way ANOVA with follow-up Tukey tests in cases where a p-value <0.05 was found. Chi-squared goodness-of-fit tests were conducted to assess group differences in categorical variables such as sex, history of hypertension, and current hypercholesteremia. All statistical analyses were conducted using MatLab's 2013b statistical package.

To assess for a relationship between WMSA stage distribution and clinical diagnosis, our final analysis staged the MCI and AD individuals using the staging cut-offs described above. Proportional differences between diagnostic groups in each stage were determined using a chi-squared goodness-of-fit test with follow-up Marascuillo tests to determine pairwise differences.

3. Results

3.1. Demographics

Demographic information for the OC individuals in each of the four quartile-based stages is listed in Table 1. Stages differed in age, with individuals in Quartile I being significantly younger than individuals in Quartiles III and IV. As designed, there was a significant increase in total WMSA burden at each progressive stage. Individuals in the four stages did not differ in MMSE, sex distribution, years of education, hypercholesteremia, history of hypertension, or history of endocrine-metabolic disorder. Individuals in Quartile I had significantly lower lateral ventricular volume than Stages II–IV. As cognitive function has been associated with WMSA burden in prior literature, we assessed if there was a correlation within-quartile or across all 97 subjects between WMSA and MMSE. No correlation was significant (Quartile I: $R = -0.09$, $p = 0.64$; Quartile II: $R = 0.21$, $p = 0.32$; Quartile III: $R = -0.11$, $p = 0.61$, Quartile IV: $R = -0.19$, $p = 0.40$).

3.2. Spatial differences across quartiles

Within-quartile means and variances of percentages of ROIs occupied by WMSA for each stage are reported in Table 2. The red, orange, and yellow colors indicate the progression cluster that the ROI belongs to. Isthmus cingulate (retrosplenial cortex) is an example of a non-

Table 1
Demographic and imaging data for individuals in each quartile. Mean and standard error of the mean values are reported for continuous measures.

Quartile	I	II	III	IV
n	25	25	25	22
WMSA load (mm³)	13,571 (425.5)	17,996 (205.7)	23,461 (478.4)	34,933 (1215)
Age	73.92 (1.2)*	74.72 (1.4)	78.4 (0.9)	79 (1.3)
Sex (% male)	40	52	40	54.55
Years education	15.44 (0.5)	15.64 (0.6)	15.8 (0.6)	15.68 (0.6)
% History hypertension	28	48	44	59
% Hypercholesteremia	12	4	16	9.1
% History endocrine-metabolic disorder	44	40	40	36.36
MMSE	29.2 (0.2)	29.24 (0.1)	29.16 (0.2)	28.82 (0.2)
Ventricular volume (% ICV)	1.6 (0.1)**	2.6 (0.2)	2.7 (0.3)	2.6 (0.3)

* Significantly different from Quartiles III & IV ($p < 0.05$).
** Significantly different from Quartiles II, III, & IV ($p < 0.05$).

Table 2
Mean and variance WMSA% values for each ROI for each of the four quartiles. For quartiles I–III, n = 25; for quartile IV, n = 22. Cells with "–" indicate that <1% of the ROI was WMSA.

	Quartile I	Quartile II	Quartile III	Quartile IV
Pars triangularis*	1.05 (0.02)	2.76 (0.036)	3.1 (0.046)	4.26 (0.065)
Precentral	1.22 (0.01)	2.49 (0.059)	3.41 (0.09)	4.55 (0.10)
Caudal MF	1.35 (0.02)	2.71 (0.03)	3.56 (0.058)	5.30 (0.062)
Temporal pole*	1.41 (0.05)	1.30 (0.033)	1.40 (0.042)	1.24 (0.038)
Isthmus cingulate*	1.51 (0.008)	1.02 (0.004)	1.52 (0.026)	1.22 (0.011)
Lingual*	2.28 (0.01)	2.73 (0.04)	2.52 (0.021)	3.71 (0.047)
Lateral Orbitofrontal*	2.52 (0.02)	2.9 (0.032)	3.03 (0.05)	3.68 (0.043)
Precuneus	2.6 (0.01)	3.05 (0.026)	4.91 (0.06)	6.92 (0.14)
Superior frontal	2.7 (0.03)	4.27 (0.057)	4.66 (0.075)	6.56 (0.14)
Pericalcarine	2.84 (0.03)	4.96 (0.15)	6.35 (0.3)	8.32 (0.25)
Rostral AC*	3.55 (0.02)	5.16 (0.055)	4.26 (0.084)	3.76 (0.058)
Insula*	3.91 (0.05)	3.67 (0.054)	3.79 (0.082)	3.58 (0.043)
Posterior cingulate*	6.35 (0.13)	5.89 (0.084)	5.78 (0.14)	5.87 (0.15)
Caudal AC*	9.09 (0.23)	10.24 (0.22)	9.12 (0.4)	8.20 (0.29)
Periventricular*	15.29 (0.08)	18.29 (0.15)	22.78 (0.37)	30.04 (0.93)
Pars opercularis*	–	1.02 (0.009)	2.15 (0.044)	2.92 (0.055)
Fusiform	–	1.08 (0.005)	1.28 (0.0063)	1.71 (0.011)
Inferior parietal*	–	1.26 (0.012)	2.47 (0.022)	4.41 (0.097)
Superior parietal	–	1.26 (0.009)	2.24 (0.029)	4.36 (0.12)
Rostral MF	–	1.53 (0.012)	2.51 (0.027)	4.01 (0.042)
Paracentral*	–	2.28 (0.074)	2.29 (0.042)	3.99 (0.12)
Banks STS*	–	–	1.17 (0.021)	1.58 (0.022)
Lateral occipital*	–	–	1.36 (0.047)	1.88 (0.041)
Postcentral*	–	–	–	1.33 (0.009)
Supramarginal*	–	–	–	2.38 (0.022)
Cuneus*	–	–	–	–
Entorhinal*	–	–	–	–
Medial Orbitofrontal*	–	–	–	–
Middle temporal*	–	–	–	–
Parahippocampal*	–	–	–	–
Inferior temporal*	–	–	–	–
Superior temporal*	–	–	–	–
Transverse Temporal*	–	–	–	–
Frontal pole*	–	–	–	–
Pars orbitalis*	–	–	–	–

STS = superior temporal sulcus, AC = anterior cingulate, MF = middle frontal.
(Red = non-scaling, orange = mid-scaling, yellow = high-scaling).
* Reliability score of at least 70% in cross-validation.

progressing cluster as its WMSA load does not change much across the four quartiles (1.51, 1.02, 1.52, and 1.22% of the total ROI volume). On the other hand, precuneus is a fast progressing cluster with the WMSA load increasing by a factor of 2.7 from quartile I to quartile IV (2.60, 3.05, 4.91, and 6.92% of total ROI volume). Fig. 2 demonstrates mean values visually; Fig. 3 shows variances and demonstrates generally low variance across ROIs suggesting consistency to the observed staging.

Individuals in Quartile I exhibited substantial WMSA in periventricular, frontal, cingulum, and medial occipital WM. Greater WMSA was found in Quartile II over Quartile I in all of these regions, with additional WMSA in rostral middle frontal, pars triangularis, pars opercularis, inferior and superior parietal, paracentral, and fusiform in Quartile II. Individuals in Quartile III had greater WMSA in all ROIs present in Quartiles I and II, with additional WMSA becoming apparent in lateral occipital and the banks of the super temporal sulcus WM. Quartile IV individuals demonstrated even more WMSA in all regions evident in Quartiles I–III, and additional WMSA was seen in supramarginal and postcentral WM. White matter in medial orbitofrontal, cuneus, entorhinal, parahippocampal, pars orbitalis, and superior, middle, and inferior temporal WM never exceeded 1% WMSA to be included as quartile-associated ROIs.

3.3. Scaling clusters

K-means clustering performed on F-statistics from one-way ANOVAs on each ROI's across-quartile WMSA measure demonstrated three distinct clusters that differentially increased in WMSA volume with increasing quartile. We deemed ROIs in the cluster with the highest F-statistic centroid to be high-scaling, those in the middle
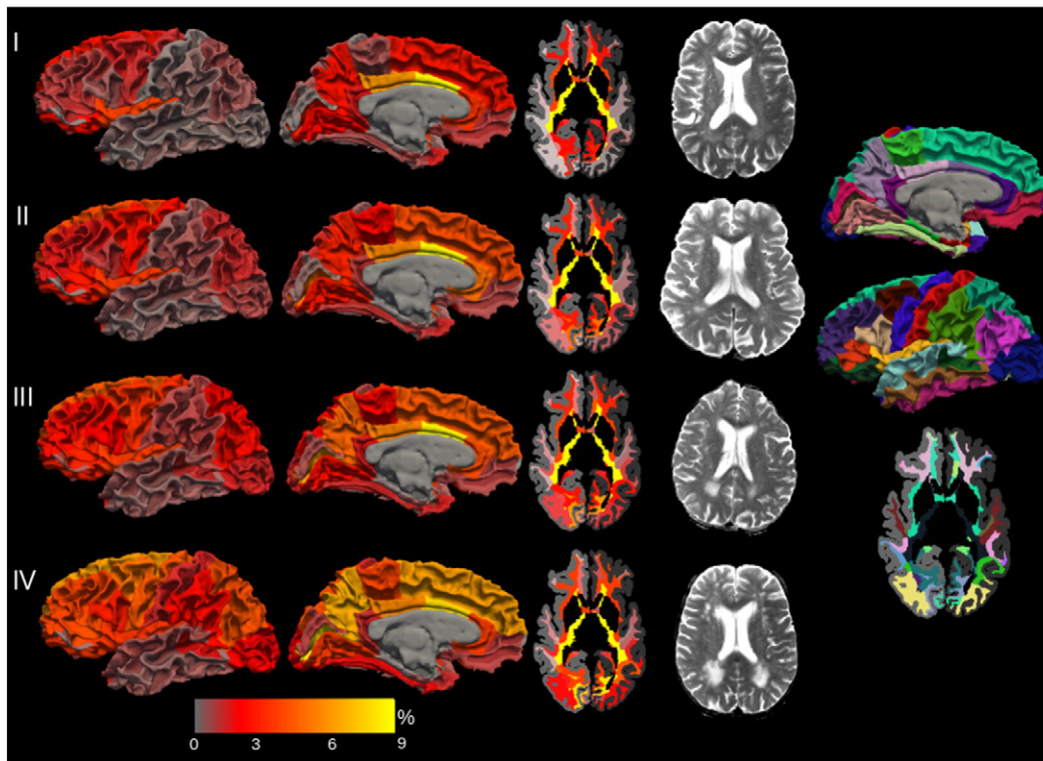
Fig. 2. Left: Spatial staging of age-associated WMSA into four quartiles, using the percent of an ROI's total WM that is occupied by WMSA as a metric for comparison across quartiles. Surface maps showing the percent of each region's underlying WM that is occupied by WMSA (first and second columns) and an axial slice through the periventricular WM showing these values in a volume view (third column) for WM disease stages I–IV. Fourth column: an example individual from each quartile, taken from the 15th position within the quartile when ordered based on total global WMSA burden. Individuals in quartile I (n = 25) demonstrate the lowest amount of global WMSA, with quartiles II and III (n = 25, n = 25) demonstrating higher global WMSA respectively, and quartile IV (n = 22) demonstrating the highest overall WMSA burden. Right: surface images and axial slice of all atlas parcellations used in the present analyses (Fischl et al., 2002; Salat et al., 2009; Desikan et al., 2006).

cluster being mid-scaling, and those in the lowest cluster to be non-scaling (Fig. 4; also denoted in Table 2).

The high-scaling cluster was composed of rostral and caudal middle frontal, inferior and superior parietal, precuneus, supramarginal, and periventricular WM. Fig. 5 shows actual progression curves along with boxplots for example ROIs from each cluster. Mean F-statistics for non-scaling, mid-scaling, and high-scaling clusters were 19.6383, 8.6318, and 1.6098, respectively. Notably, several ROIs did not have >1% WMSA until Quartiles III or IV; supramarginal WM in the high-scaling cluster, and the postcentral and banks of the superior temporal sulcus WM in the mid-scaling cluster (dark regions in Fig. 4). All high-scaling regions followed a more non-linear trajectory than mid-scaling regions, with greater amounts of WMSA increase occurring at each increasing quartile.

Noting the high variance in inferior parietal WMSA in Quartile IV individuals, we conducted a separate follow-up analysis using these 22 individuals to determine if the overall spatial pattern of WMSA differed between those with high (n = 11) and low (n = 11) inferior parietal WMSA. We determined the mean WMSA volume percent in each ROI for these two new subgroups, and subtracted the ROI-based mean values of the low inferior parietal WMSA individuals from the high inferior parietal WMSA individuals. These two splits did not differ in age, sex distribution, history of hypertension, hypercholesteremia, or endocrine-metabolic disease. In the 'high' split individuals, WMSA volume percent was on average 7.84% higher in the periventricular WM, 4.5% higher in the inferior parietal WM, 3.7% higher in the precuneus WM, 2.3% higher in the paracentral WM, and 2% higher in the posterior and caudal anterior cingulate WM, but <0.5% higher in all other ROIs. These reflect the regions that demonstrated the highest degrees of variance across all quartiles. Importantly, the mean WMSA burdens of all of

these regions in the 'low' split Quartile IV individuals were still higher than the means in the Quartile III individuals.

3.4. Cluster validation

Reliability of these clusters was determined by performing 10,000 iterations of the quartiling and clustering technique with subsamples of the data. Twenty-seven of the 35 ROIs had reliability scores over 70% (starred ROIs in Table 2). All other ROIs had a reliability score above 60% with the exception of caudal middle frontal WM, whose score was 50.1%, and was equally assigned to mid-scaling and high-scaling.

Periventricular WM demonstrated the highest F-statistic in the true data (26.1293) and was first tested for significance. Using the ROI-shuffling method, none of the 10,000 iterations produced a maximum F-statistic higher than 26.1293 and periventricular WMSA was deemed to be a significantly high-scaling ROI at $p < 0.0001$. For the remaining high-scaling ROIs, only two or fewer shuffling iterations generated an F-statistic higher than that generated for the true data, and therefore the F-statistics for all high-scaling ROIs are significant at $p < 0.0002$. These p-values are not corrected for multiple comparisons; however, they are so significant that they would still be significant even Bonferroni correction across the 70 ROIs.

3.5. Cut-off based staging

For this final staging using ROI cut-off values, all individuals were considered for inclusion in any stage. Cut-off values for stage inclusion were based on the seven ROIs deemed high-scaling in the quartile-based staging, and a flowchart of this process is shown in Fig. 6. The supramarginal WM showed the greatest difference between the third
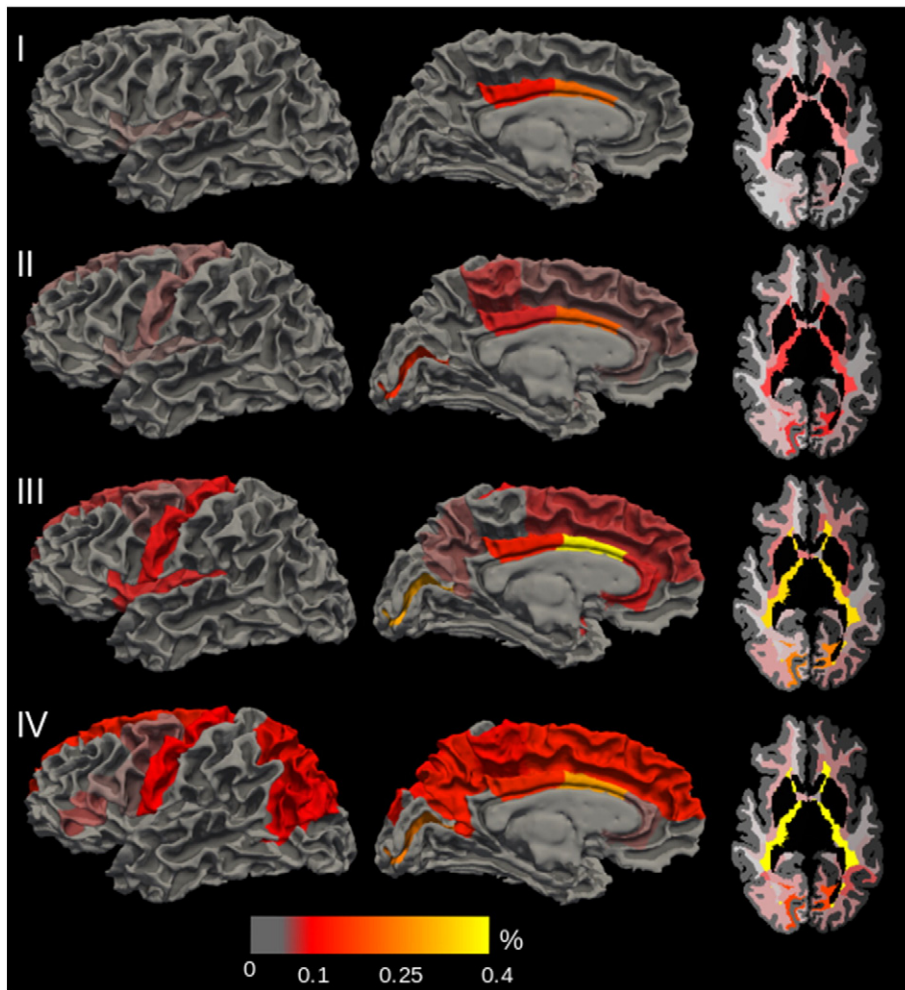
Fig. 3. Within-quartile variance maps of the volume percent of WMSA in each ROI. Colorbar represents within-ROI variance in terms of the percent of the ROI. Values are reported in Table 2.
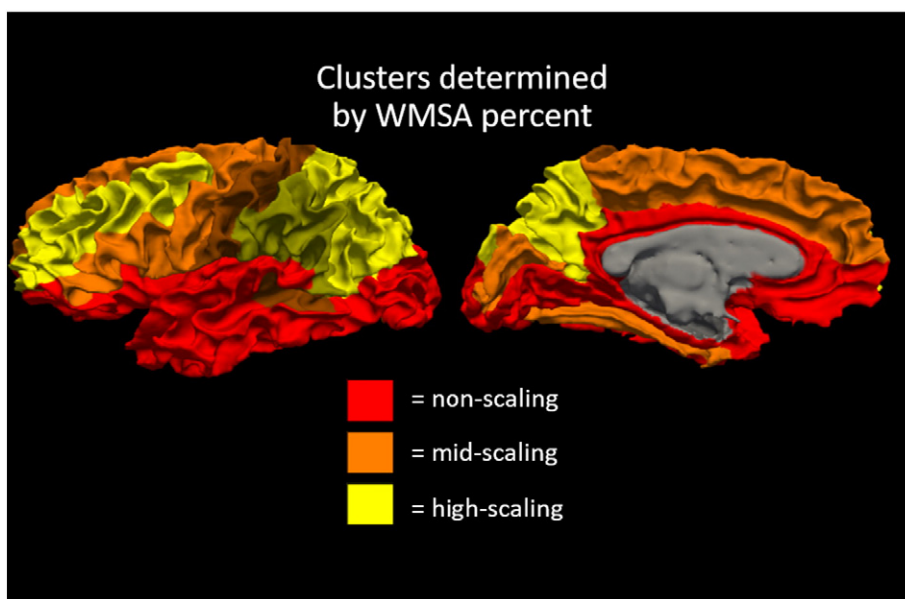

Fig. 4. Surface maps depicting which scaling cluster each region's underlying WM belongs to, with respect to WMSA percent of total ROI WM (WMSA percent), as determined by statistically different WMSA measurements across all four quartiles of WMSA burden. Scaling here refers to the strength of the statistical significance when assessing WMSA burden across the four quartiles for a given region, where "high-scaling" indicates that the increase in regional WMSA with increasing quartile is highly significant.
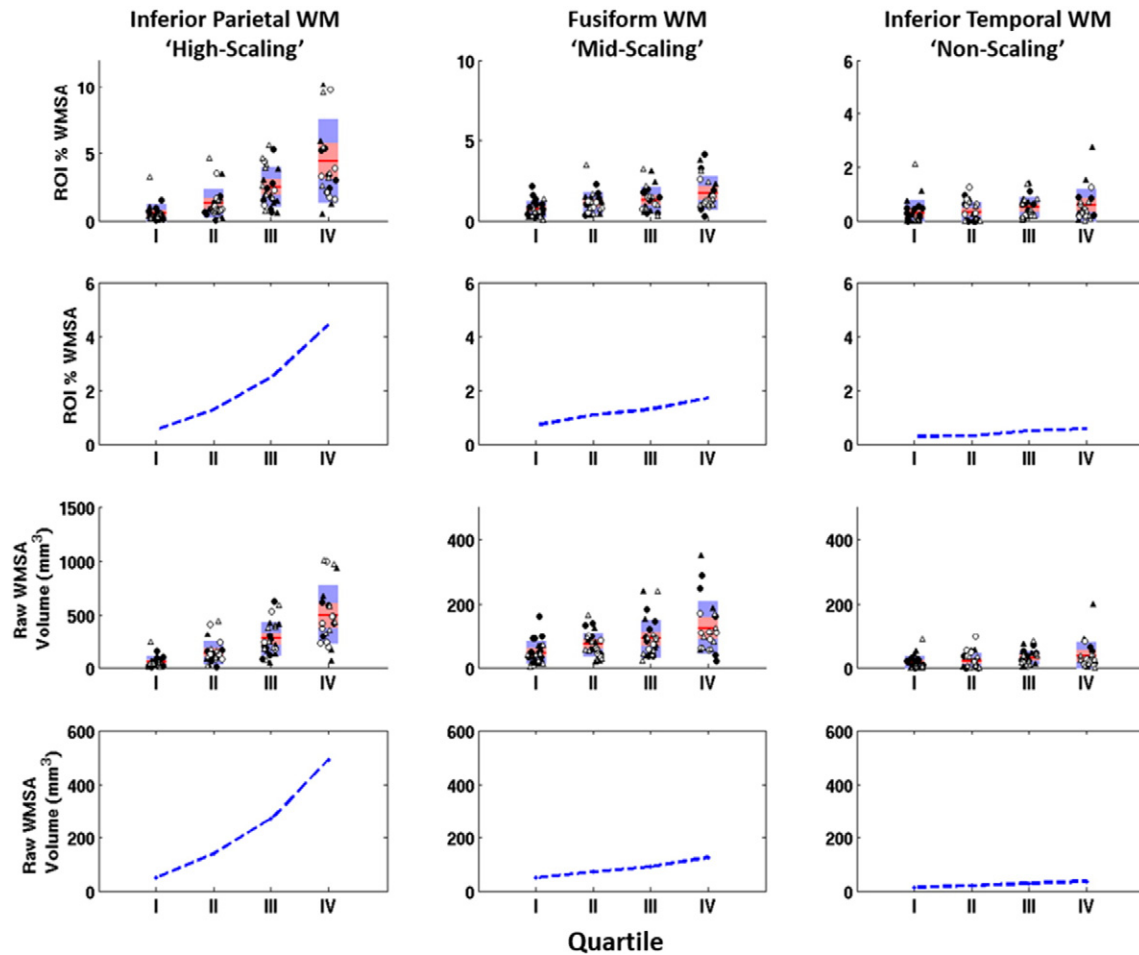
Fig. 5. Left column: Individual subject data across all 4 quartiles showing the percent of the total WM occupied by WMSA in the inferior parietal region (top); a scaling curve for percent WMSA created by plotting mean values per quartile (second); individual raw WMSA volumes across the 4 quartiles in inferior parietal WM (third); a scaling curve for raw WMSA volume (bottom) (Individual data points: white = hypertensive, black = non-hypertensive, circle = male, triangle = female; red: mean, pink: 95% confidence interval of the mean; blue: 1 standard deviation). Middle column: Same data shown for fusiform WM, a mid-scaling region. Right column: Same data shown for inferior temporal WM, a non-scaling region.
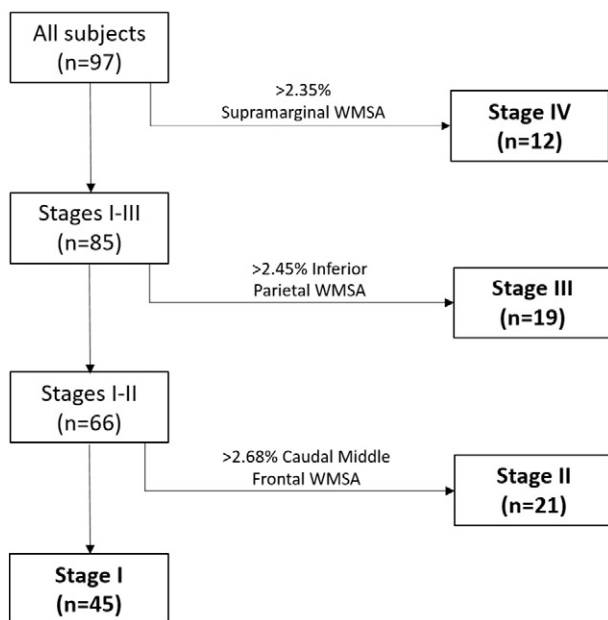

Fig. 6. Flowchart demonstrating cut-off values for inclusion criteria for final staging in OC individuals, based on values derived from quartile-based staging.

and fourth quartiles as determined by a *t*-test. Using the mean and standard deviation values reported in Table 2, a cut-off of one standard deviation below the mean of the fourth quartile (2.35%) was chosen and any individual with supramarginal WMSA above this amount was placed in Stage IV. Next, the remaining individuals were placed into Stage III based on an inferior parietal WMSA cut-off of one standard deviation below the mean of third quartile inferior parietal WMSA (2.45%). Finally, the remaining individuals were placed in Stage II based on a caudal middle frontal WMSA cut-off of one standard deviation below the mean of second quartile caudal middle frontal WMSA (2.68%).

Demographics for the individuals in final cut-off based staging are presented in Supplementary Table 1 along with mean and variance values for the seven high-scaling clusters determined in the first part of the study. Individuals in these final stages did not differ significantly in age or MMSE, but they did differ in hypertension, with a greater proportion of individuals in increasing stages having hypertension. Furthermore, mean WMSA values for each ROI showed a similar spatial pattern across the four quartile-based stages as with the four final stages (Supplementary Fig. 1), but within-ROI variance significantly decreased in several ROIs across all stages (Supplementary Fig. 2), indicating greater similarity between individuals in each final stage.

3.6. Staging across diagnostic group

Using the staging cut-off values, we then staged our MCI and AD groups. Individuals in these groups did not differ significantly in age,
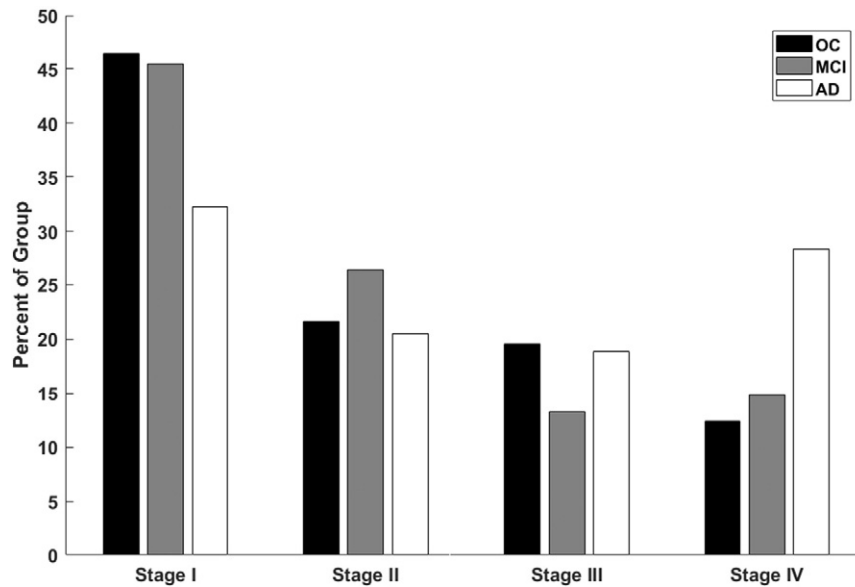
Fig. 7. Within-group percentages of individuals in each WMSA Stage using secondary staging cut-off values across three diagnostic groups. Significant differences were found between AD and MCI and between AD and OC in Stages I and IV.

education, or history of cardiovascular risk factors nor did they differ from the OC group. Results of the percent of individuals in each group and stage are shown in Fig. 7. A chi-squared goodness-of-fit test indicated that within-stage percentages were different across the three diagnostic groups ($\chi^2 = 15.4490$, $p = 0.017$) and follow-up Marascuillo test for multiple comparisons demonstrated that significant differences were between AD and MCI, and AD and OC, in Stages I and IV ($p < 0.01$). As expected, the greatest percentage of the AD group fell into Stage IV, and the greatest percentage of the OC group fell into Stage I. Demographic data for these three diagnostic groups is presented in Supplementary Table 2.

4. Discussion

We present here a regional staging of age-associated WMSA based on MRI measures of WMSA quantified by their proximity to cortical landmarks. We demonstrate that the regional scaling of WMSA to global burden, which we infer is due to the pathologic course of white matter disease, follows a consistent spatial pattern in cognitively healthy older adults, implying differential regional vulnerability to disease. Individuals with AD then showed an increase in prevalence in Stage IV over both OC and MCI groups, as well as a decrease in prevalence in Stage I. These results also emphasize the need to better understand the factors that contribute to the pathophysiology of WMSA in older adults and diseases of aging. Collectively, this information may lead to a better understanding of the mechanisms contributing to age-associated WMSA and how this tissue damage compromises neurological function and clinical status in older adults.

As in post-mortem studies (Braak and Braak, 1991; Augustinack et al., 2012; Arnold et al., 1991), the current work used single time point data to infer stages based on the examination of accumulating regional pathology. In contrast to prior work, we used the global burden of WMSA as a metric of overall disease and used this to determine the regional profile with increasing total lesion volume. Given that WMSA do not decrease or shrink in the context of aging (Erten-Lyons et al., 2013; Schmidt et al., 1999), we infer here that this regional scaling is linked to progression of disease burden. The results therefore suggest that in cognitively healthy aging, WMSA originate in periventricular WM as well as the WM underlying caudal frontal, superior frontal, precuneus, and cingulum gray matter. Secondary progression includes inferior parietal, occipital, and some medial temporal regions, followed by WMSA

progression to superior parietal WM, and finally supramarginal WM. We observe a general sparing of lateral temporal, orbitofrontal, cuneus, parahippocampal, and entorhinal WM. It is interesting to note that these spared regions are regions that are known to be susceptible to classical Alzheimer's neurofibrillary pathology (Braak and Braak, 1991). It is therefore possible that regions showing rapid accumulation of white matter disease may have a particularly appreciable influence on cognitive status as a "second hit" (Provenzano et al., 2013; Zlokovic, 2014) to regions being used in a compensatory manner to overcome the primary neurodegenerative deficits. This speculative idea will be examined in future work.

The seven regions that were clustered as high-scaling with global burden were inferior and superior parietal, supramarginal, precuneus, periventricular, and caudal and rostral middle frontal WM. This pattern was found to be highly unlikely by chance using a permutation test. The pattern persisted when using a random subsampling of the total subject pool. Of great significance is that these regions align to known cerebrovascular boundary zones (also known as watershed regions), which are areas that are at the border of blood supply zones from two different major cerebral arteries and are thus most susceptible to hypoperfusion (Damasio, 1983; Haines, 1995). Furthermore, these regions are in close proximity to cortical regions in which cerebral blood flow (CBF) is known to decrease with advancing age (Chen et al., 2011). The relationship between reductions in WM integrity and reductions in cortical CBF have also been demonstrated (Brickman et al., 2009a; Chen et al., 2013), supporting the idea that these high-scaling regions may be tightly linked to neighboring cortical perfusion changes. We conclude that the spatial patterns and degree of accumulation of WMSA across the defined stages are due to common age-associated processes including decrements in vascular health. However, we note that common clinical indicators such as 'hypertension' are not particularly sensitive to detecting this burden based on WMSA staging.

A portion of the regions examined appear to be inevitably affected by WMSA, even in the early stages, but do not show increases in WMSA with increasing global burden and were categorized as non-scaling. These regions include the cingulum, insular, inferior frontal, and pericalcarine regions. A subset of the non-scaling regions also appear to be protected entirely from WMSA, including the lateral temporal, lateral orbitofrontal, cuneus, entorhinal and parahippocampal WM. Interestingly, these areas have been shown to have a dual-blood supply (Moody et al., 1990). A dual-blood supply decreases a region's

susceptibility to hypoperfusion, and therefore may explain why these regions do not show increased damage with increased global WMSA.

High-scaling regions were used to determine cut-off values for 'final' staging of individuals. This method provided a non-quartile-based procedure for assigning individuals to WMSA stage, yet it followed a similar pattern of spatial WMSA development. Furthermore, increases in hypertension with increasing stage were observed using this staging method, reflecting the extensive histological and epidemiological literature that has shown links between hypertension and WM integrity (Erten-Lyons et al., 2013; van Swieten et al., 1991), and regions of WM damage are often due to hypoperfusion of the surrounding tissue (Pantoni and Garcia, 1997; Bernbaum et al., 2015; Moody et al., 2004). Studies have demonstrated hypoperfusion in normal-appearing white matter that precedes the development of WMSA (O'Sullivan et al., 2002). Due to the differing levels of perfusion throughout the WM, it is likely that different WM regions become damaged at different rates, depending on the regional susceptibility to hypoperfusion (Moody et al., 1990). In addition to the differences in physiological factors across secondary stages seen in the older controls, we demonstrated increased prevalence of AD in Stage IV over controls and individuals with MCI, as well as a decrease in prevalence of AD in Stage I. While it has been shown before that individuals with AD have a greater global WMSA burden than OC and MCI individuals, no regional WMSA staging mechanism has existed prior to this study that demonstrates a similar ability to separate these diagnoses.

Overall, the current data demonstrate a regionally stereotyped increase in WMSA with increasing overall burden in cognitively healthy older adults. Cut-off values for supramarginal, inferior parietal, and caudal middle frontal WMSA have been proposed as staging guidelines, and these values demonstrated a decrease in within-stage variance than the quartile-based staging, as well as some relevant indication of disease stage. Information from this work will guide future efforts towards a better understanding of the impact of WMSA on functional properties of the brain and normal cognitive and behavioral variation in older adults.

Funding

Appendix A. Supplementary data

Supplementary data to this article can be found online at http://dx.doi.org/10.1016/j.nicl.2017.01.022.

References

Arnold, S.E., Hyman, B.T., Flory, J., et al., 1991. The topographical and neuroanatomical distribution of neurofibrillary tangles and neuritic plaques in the cerebral cortex of patients with Alzheimer's disease. Cereb. Cortex 1 (1), 103–116.

Augustinack, J.C., Huber, K.E., Postelnicu, G.M., et al., 2012. Entorhinal verrucae geometry is coincident and correlates with Alzheimer's lesions: a combined neuropathology and high-resolution ex vivo MRI analysis. Acta Neuropathol. 123 (1), 85–96.

Benedictus, M.R., Binnewijzend, M.A.A., Kuijer, J.P.A., et al., 2014. Brain volume and white matter hyperintensities as determinants of cerebral blood flow in Alzheimer's disease. Neurobiol. Aging 35 (12), 2665–2670.

Bernbaum, M., Menon, B.K., Fick, G., et al., 2015. Reduced blood flow in normal white matter predicts development of leukoaraiosis. J. Cereb. Blood Flow Metab. 35 (10), 1610–1615.

Braak, H., Braak, E., 1991. Neuropathological stageing of Alzheimer-related changes. Acta Neuropathol. 82 (4), 239–259.

Brickman, A.M., Zahra, A., Muraskin, J., et al., 2009a. Reduction in cerebral blood flow in areas appearing as white matter hyperintensities on magnetic resonance imaging. Psychiatry Res. 172 (2), 117–120.

Brickman, A.M., Muraskin, J., Zimmerman, M.E., 2009b. Structural neuroimaging in Alzheimer's disease: do white matter hyperintensities matter? Dialogues Clin. Neurosci 11 (2), 181–190.

Chen, J.J., Rosas, H.D., Salat, D.H., 2011. Age-associated reductions in cerebral blood flow are independent from regional atrophy. NeuroImage 55 (2), 468–478.

Chen, J.J., Rosas, H.D., Salat, D.H., 2013. The relationship between cortical blood flow and sub-cortical white-matter health across the adult age span. PLoS One 8 (2), e56733.

Dale, A.M., Sereno, M.I., 1993. Improved localizaction of cortical activity by combining EEG and MEG with MRI cortical surface reconstruction: a linear approach. J. Cogn. Neurosci. 5 (2), 162–176.

Dale, A.M., Fischl, B., Sereno, M.I., 1999. Cortical surface-based analysis. I. Segmentation and surface reconstruction. NeuroImage 9 (2), 179–194.

Damasio, H., 1983. A computed tomographic guide to the identification of cerebral vascular territories. Arch Neurol 40 (3), 138–142.

de Groot, J.C., de Leeuw, F.E., Oudkerk, M., et al., 2001. Cerebral white matter lesions and subjective cognitive dysfunction: the Rotterdam scan study. Ann. Neurol. 56 (11), 1539–1545.

de Groot, J.C., de Leeuw, F.E., Oudkerk, M., et al., 2002. Periventricular cerebral white matter lesions predict rate of cognitive decline. Ann. Neurol. 52 (3), 335–341.

de Leeuw, F.E., de Groot, J.C., Achten, E., et al., 2001. Prevalence of cerebral white matter lesions in elderly people: a population based magnetic resonance imaging study. The Rotterdam scan study. J. Neurol. Neurosurg. Psychiatry 70 (1), 9–14.

DeCarli, C., Massaro, J., Harvey, D., et al., 2005. Measures of brain morphology and infarction in the Framingham heart study: establishing what is normal. Neurobiol. Aging 26 (4), 491–510.

Desikan, R.S., Segonne, F., Fischl, B., et al., 2006. An automated labeling system for subdividing the human cerebral cortex on MRI scans into gyral based regions of interest. NeuroImage 31, 968–980.

Dufouil, C., de Kersaint-Gilly, A., Besancon, V., et al., 2001. Longitudinal study of blood pressure and white matter hyperintensities: the EVA MRI cohort. Neurology 56 (7), 921–926.

Erten-Lyons, D., Woltjer, R., Kaye, J., et al., 2013. Neuropathologic basis of white matter hyperintensity accumulation with advanced age. Neurology 81 (11), 977–983.

Fazekas, F., Chawluk, J.B., 1987. Alavi a. MR signal abnormalities at 1.5 T in Alzheimer's dementia and normal aging. Am. J. Neuroradiol. 8 (3), 421–426.

Fazekas, F., Niederkron, K., Schmidt, R., et al., 1988. White matter signal abnormalities in normal individuals: correlation with carotid ultrasonography, cerebral blood flow measurements, and cerebrovascular risk factors. Stroke 19 (10), 1285–1288.

Fischl, B., Dale, A.M., 2000. Measuring the thickness of the human cerebral cortex from magnetic resonance images. Proc. Natl. Acad. Sci. USA 97 (20), 11050–11055.

Fischl, B., Sereno, M.I., Tootell, R.B.H., Dale, A.M., 1999. High-resolution intersubject averaging and a coordinate system for the cortical surface. Hum. Brain Mapp. 8 (4), 272–284.

Fischl, B., Liu, A., Dale, A.M., 2001. Automated manifold surgery: constructing geometrically accurate and topologically correct models of the human cerebral cortex. IEEE Trans. Med. Imaging 20 (1), 70–80.

Fischl, B., Salat, D.H., Busa, E., et al., 2002. Whole brain segmentation: automated labeling of neuroanatomical structures in the human brain. Neuron 33 (3), 341–355.

Fischl, B., Van Der Kouwe, A., Destrieux, C., et al., 2004a. Automatically parcellating the human cerebral cortex. Cereb. Cortex 14, 11–22.

Fischl, B., Salat, D.H., Van Der Kouwe, A., et al., 2004b. Sequence-independent segmentation of magnetic resonance images. NeuroImage 23 (Suppl. 1), S69–S84.

Frisoni, G.B., Galluzzi, S., Pantoni, L., Filippi, M., 2007. The effect of white matter lesions on cognition in the elderly — small but detectable. Nat. Clin. Pr. Neurol. 3 (11), 620–627.

Grueter, B.E., Schulz, U.G., 2012. Age-related cerebral white matter disease (leukoaraiosis): a review. Postgrad. Med. J. 88 (1036), 79–87.

Haines, D.E., 1995. Neuroanatomy: An Atlas of Structures, Sections, and Systems. second ed. Urban and Schwarzenberg, Baltimore.

Han, X., Jovicich, J., Salat, D., et al., 2006. Reliability of MRI-derived measurements of human cerebral cortical thickness: the effects of field strength, scanner upgrade and manufacturer. NeuroImage 32 (1), 180–194.

Iadecola, C., 2013. The pathobiology of vascular dementia. Neuron 80 (4), 844–866.

Jack, C.R., Bernstein, M.A., Fox, N.C., et al., 2008. The Alzheimer's disease neuroimaging initiative (ADNI): MRI methods. J. Magn. Reson. Imaging 27 (4), 685–691.

Jovicich, J., Czanner, S., Greve, D., et al., 2006. Reliability in multi-site structural MRI studies: effects of gradient non-linearity correction on phantom and human data. NeuroImage 30 (2), 436–443.

Lindemer, E.R., Salat, D.H., Smith, E.E., et al., 2015. White matter signal abnormality quality differentiates mild cognitive impairment that converts to Alzheimer's disease from nonconverters. Neurobiol. Aging 36 (9), 2447–2457.

Longstreth Jr., W.T., 1998. Brain abnormalities in the elderly: frequency and predictors in the United States (the Cardiovascular Health Study). Cardiovascular Health Study Collaborative Research Group. J. Neural Transm. 53 (Suppl), 9–16 (0303–6995 (Print)).

Maillard, P., Fletcher, E., Lockhart, S.N., et al., 2014. White matter hyperintensities and their penumbra lie along a continuum of injury in the aging brain. Stroke 45 (6), 1721–1726.

Moody, D.M., Bell, M.A., Challa, V.R., 1990. Features of the cerebral vascular pattern that predict vulnerability to perfusion or oxygenation deficiency: an anatomic study. Am. J. Neuroradiol. 11 (3), 431–439.

Moody, D.M., Thore, C.R., Anstrom, J.A., et al., 2004. Quantification of afferent vessels shows reduced brain vascular density in subjects with leukoaraiosis. Radiology 233 (3), 883–890.

O'Sullivan, M., Lythgoe, D.J., Pereira, A.C., et al., 2002. Patterns of cerebral blood flow reduction in patients with ischemic leukoaraiosis. Neurology 59 (3), 321–326.

Pantoni, L., Garcia, J.H., 1997. Pathogenesis of leukoaraiosis: a review. Stroke 28 (3), 652–659.

Provenzano, F., Muraskin, J., Tosto, G., et al., 2013. White matter hyperintensities and cerebral amyloidosis: necessary and sufficient for clinical expression of Alzheimer disease? JAMA Neurol. 70 (4), 455–461.

Salat, D.H., Greve, D.N., Pacheco, J.L., et al., 2009. Regional white matter volume differences in nondemented aging and Alzheimer's disease. NeuroImage 44 (4), 1247–1258.

Scheltens, P., Barkhof, F., Leys, D., et al., 1993. A semiquantative rating scale for the assessment of signal hyperintensities on magnetic resonance imaging. J. Neurol. Sci. 114 (1), 7–12.

Schmidt, R., Fazekas, F., Kapeller, P., et al., 1999. MRI white matter hyperintensities: three-year follow-up of the Austrian stroke prevention study. Neurology 53 (1), 132–139.

Spilt, A., Goekoop, R., Westendorp, R.G.J., et al., 2006. Not all age-related white matter hyperintensities are the same: a magnetization transfer imaging study. AJNR Am. J. Neuroradiol. 27 (9), 1964–1968.

van Swieten, J.C., van den Hout, J.H., van Ketel, B.A., et al., 1991. Periventricular lesions in the white matter on magnetic resonance imaging in the elderly. A morphometric correlation with arteriolosclerosis and dilated perivascular spaces. Brain 114 (2), 761–774.

Wardlaw, J.M., Smith, E.E., Biessels, G.J., et al., 2013a. Neuroimaging standards for research into small vessel disease and its contribution to ageing and neurodegeneration. Lancet Neurol. 12 (8), 822–838.

Wardlaw, J.M., Smith, C., Dichgans, M., 2013b. Mechanisms of sporadic cerebral small vessel disease: insights from neuroimaging. Lancet. Neurol. 12 (5), 483–497.

Wei, X., Warfield, S.K., Zou, K.H., et al., 2002. Quantitative analysis of MRI signal abnormalities of brain white matter with high reproducibility and accuracy. J. Magn. Reson. Imaging 15 (2), 203–209.

Yoshita, M., Fletcher, E., Harvey, D., et al., 2006. Extent and distribution of white matter hyperintensities in normal aging, MCI, and AD. Neurology 67 (12), 2192–2198.

Zimmerman, R.D., Fleming, C.A., Lee, B.C., et al., 1986. Periventricular hyperintensity as seen by magnetic resonance: prevalence and significance. AJ. Am. J. Roentgenol. 146 (3), 443–450.

Zlokovic, B., 2014. Neurovascular Pathways to Neurodegeneration in Alzheimer's Disease and Other Disorders. 12 (12) pp. 723–738.